Nuclear Instruments and Methods in Physics Research A ∎ (∎∎∎∎) ∎∎∎–∎∎∎

Contents lists available at ScienceDirect

Nuclear Instruments and Methods in Physics Research A

journal homepage: www.elsevier.com/locate/nima

AREAL low energy electron beam applications in life and materials sciences

V.M. Tsakanov [a,b,*], R.M. Aroutiounian [b], G.A. Amatuni [a], L.R. Aloyan [b], L.G. Aslanyan [b], V.Sh. Avagyan [a], N.S. Babayan [b,c], V.V. Buniatyan [d], Y.B. Dalyan [a], H.D. Davtyan [a], M.V. Derdzyan [f], B.A. Grigoryan [a], N.E. Grigoryan [e], L.S. Hakobyan [a], S.G. Haroutyunian [b], V.V. Harutiunyan [e], K.L. Hovhannesyan [f], V.G. Khachatryan [a], N.W. Martirosyan [a,d], G.S. Melikyan [d], A.G. Petrosyan [f], V.H. Petrosyan [a], A.A. Sahakyan [e], V.V. Sahakyan [a], A.A. Sargsyan [a], A.S. Simonyan [a], S.Sh. Tatikyan [a], G.V. Tsakanova [c], E. Tsovyan [b], A.S. Vardanyan [a], V.V. Vardanyan [a], A.S. Yeremyan [a], H.N. Yeritsyan [e], G.S. Zanyan [a]

[a] CANDLE Synchrotron Research Institute, 0040 Yerevan, Armenia
[b] Yerevan State University, 0025 Yerevan, Armenia
[c] Institute of Molecular Biology NAS, 0014 Yerevan, Armenia
[d] State Engineering University of Armenia, 0009 Yerevan, Armenia
[e] A.I. Alikhanyan National Science Laboratory (YerPhi), 0036 Yerevan, Armenia
[f] Institute for Physical Research NAS, 0203 Ashtarak, Armenia

ARTICLE INFO

Keywords:
Accelerator
Photogun
Electron beam
Irradiation

ABSTRACT

The AREAL laser-driven RF gun provides 2–5 MeV energy ultrashort electron pulses for experimental study in life and materials sciences. We report the first experimental results of the AREAL beam application in the study of molecular-genetic effects, silicon-dielectric structures, ferroelectric nanofilms, and single crystals for scintillators.

© 2016 Published by Elsevier B.V.

1. Introduction

The Advanced Research Electron Accelerator Laboratory (AREAL) is a laser-driven radio-frequency (RF) gun based linear accelerator project designed as a multipurpose facility in the fields of new accelerator technology and applied research [1,2]. The facility first stage, RF photogun, provides a 2–5 MeV energy electron beam with bunch charge of 10–250 pC. The usage of the AREAL electron beams in the fields of life and materials sciences is an important issue for exploiting the facility's full potential and its development. Although the advanced experimental techniques at the new facility, like relativistic electron diffraction [3], are under development, the experimental investigations in the fields of radiobiology, molecular physics, solid-state physics, and microelectronics are claimed. In this paper a short review of the AREAL performance and the first experimental results in life and materials sciences are presented.

2. AREAL facility and experimental set-ups

The basic aim of the AREAL facility is the generation and acceleration of ultrashort electron bunches with small transverse emittances. The main peculiarities of the AREAL facility are the relatively broad range of beam parameters variation and stable machine operation within this range. The design specification of the facility implies the usage of the metallic photocathode and an ultrafast UV laser. The choice of the metalic (copper) photocathode is stipulated by a high-damage threshold (100 mJ/cm^2), short response time (<0.02 ps) and a long lifetime ($\sim$1 year) that provide the facility reliable operation with sub-picosecond electron pulses at the gun exit. The RF gun is driven by the Yb doped laser system capable to provide about 200 μJ energy at 258 nm wavelength and 0.4–9 ps pulse duration. The main parameters of the AREAL laser system and electron beam are presented in Tables 1 and 2, respectively.

The diagnostic tools include the magnetic spectrometer, Faraday cups, YAG screens, and pepper port for the beam energy, energy spread, charge, beam profile, emittance measurements, and control.

* Corresponding author.
E-mail address: tsakanov@asls.candle.am (V.M. Tsakanov).

http://dx.doi.org/10.1016/j.nima.2016.02.028
0168-9002/© 2016 Published by Elsevier B.V.

The facility schematic layout is presented in Fig. 1. The machine set-up provides a good basis for the facility development and the start-up of the first experiments. The facility has two in-air experimental stations H1 and H2 for applied research in the fields of life and materials sciences. The first station H1 with a focused electron beam is located downstream of the linac. The second station H2 is designated for the electron energy correlated experiments and is located after the magnetic spectrometer in order to avoid the dark current effects. The beam profiles at the experimental stations H1 and H2 are presented in Fig. 2. The experimental stations are separated from the accelerator vacuum chamber (~1 nTorr vacuum) by special Titanium windows.

3. Bio-medical applications

Innovative experimental in vitro investigations in radiobiology are of crucial importance for understanding the basic mechanisms of radiation damage of the cell [4–7]. The 2–5 MeV energy AREAL ultrashort electron bunches are a very appropriate tool for precise and controllable studies in radiation biology and medical physics in a wide range of applied radiation doses.

Table 1
UV laser parameters.

Wavelength (nm)	258
Pulse energy (μJ)	200
Repetition rate (Hz)	1–100
Energy stability	< 2%
Beam divergence (mrad)	< 0.3
Beam diameter (mm)	4.0

Table 2
AREAL beam parameters.

Energy (MeV)	2–5
Bunch charge (pC)	10–250
Bunch length (ps)	0.4–9
Norm. emittance (mm-mrad)	< 0.5
RMS energy spread	< 1.5%
Repetition rate	1–50 Hz

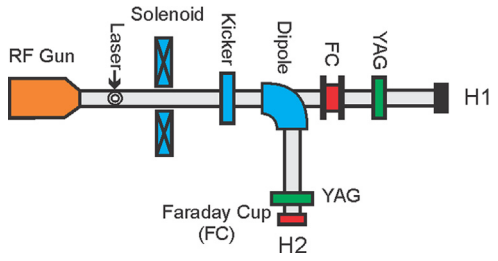

Fig. 1. AREAL RF photogun layout with experimental stations H1 and H2.

3.1. Genetic effects. DNA radiation damage and repair

The dose–response effects of reparable and non-reparable DNA damages induced by the AREAL electron beams have been studied. The first step toward the application of electron beams in radiobiology is the development of biodosimetry based on molecular-genetic effects of radiation on DNA as a principal biological target for the radiation damaging action.

To estimate the level of primary DNA damage, as well as the repairable and non-repairable DNA damages, after cell irradiation the comet assay (single cell gel electrophoresis) was carried out under alkaline conditions [8]. The study of irradiation-induced primary DNA damage was performed by comet assay of the cells which after irradiation were kept for 3 h under dark and cold conditions to prevent DNA repair. Repairable and non-repairable DNA damages were assessed after 24 h-incubation of irradiated cell culture in complete growth medium at 37 °C. The level of DNA damage was defined by the tail moment given as the relative amount of DNA in the tail of the comet multiplied by the median migration distance.

The exposure of K562 human chronic myelogenic leukemia cells to ultrafast electron irradiation at different doses revealed the dose-dependent increase of the primary DNA damage. Fig. 3 represents the comets images (qualitative data of primary DNA damage) 3 h after irradiation. Non-irradiated cells appeared as spherical nucleoids with no DNA migration (Fig. 3a). All cells were examined and captured using a fluorescent microscope at 400 × magnification. The low dose of irradiation (2 Gy) leads to the formation of few strand breaks (Fig. 3b), while doses of 4 Gy, 8 Gy and 16 Gy generate significant increase of strand breaks as compared to control. These cells have a long tail of DNA streaming out of the nucleoid and form a comet-like appearance (Fig. 3c–f). A significant increase in DNA strand breaks 3 h after the irradiation was observed at all doses applied (Fig. 4). Meanwhile, the decrease of DNA damage level at doses higher than 4 Gy is revealed. This observation may be due to the loss of highly damaged non-viable cells from the population, which results in a lower level of DNA damage in the remaining viable cells. After 24 h of cell incubation, the damaged DNAs have repaired up to irradiation dose of 24 Gy (Fig. 4). The increased level of DNA damage after 24 h of incubation at 24 Gy irradiation dose can indicate the increase of viable cells population with a higher level of damage.

It is known that there are qualitative differences between the low and high linear energy transfer (LET) radiation both in

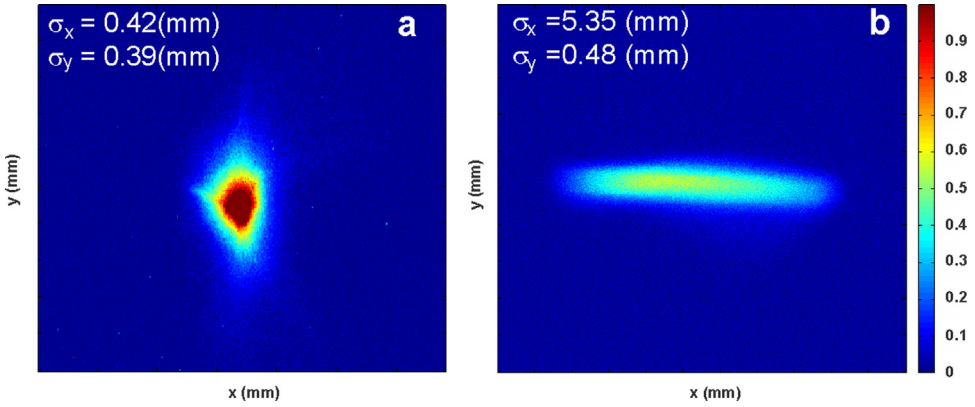

Fig. 2. Electron beam transverse profiles at experimental stations H1 (a) and H2 (b).

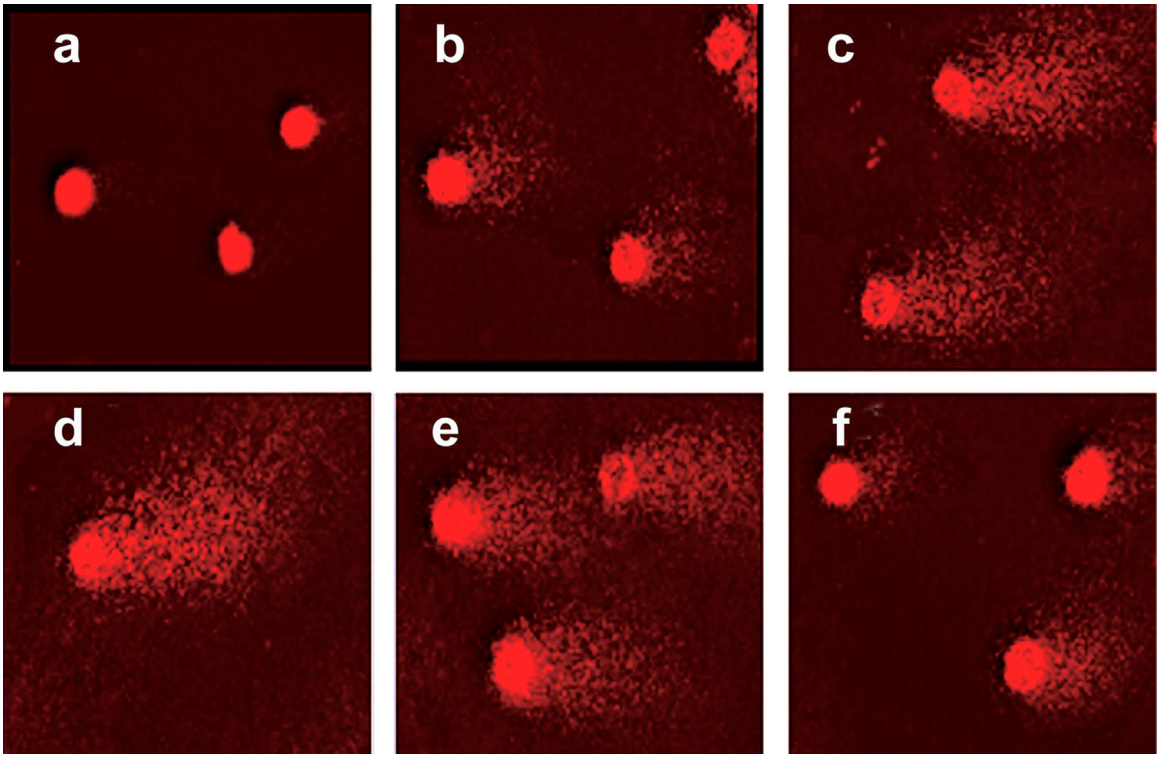

Fig. 3. Comet assay images of K562 cells before (a) and 3 h after irradiation (b) dose 2 Gy, (c) 4 Gy, (d) 8 Gy, (e) 16 Gy, and (f) 24 Gy.

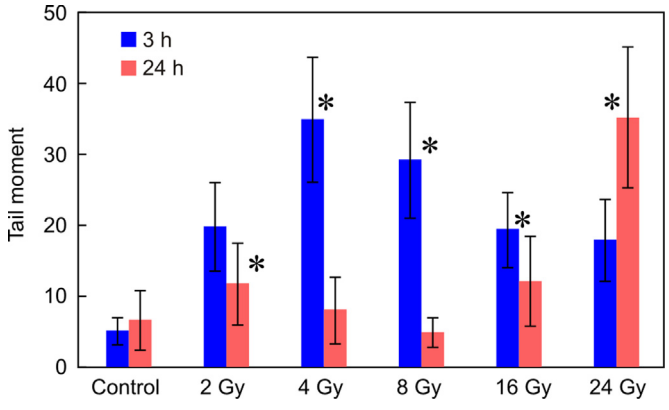

Fig. 4. Comparison between levels of DNA damage 3 and 24 h after irradiation.

induction and in repair of DNA damage [9–11]. It was shown that electrons, as a source of low LET radiation, led to isolated DNA lesions, including single-strand and double-strand breaks of DNA, which were generally repaired efficiently. The prolonged irradiation has a cumulative effect with complex DNA lesions, which are more difficult to repair than isolated lesions. Those complex DNA lesions are considered to be the key precursors of most early and late effects of radiation, associated with the increased relative biological effectiveness [12].

3.2. Radiation therapy. DNA damage in the presence of porphyrins

Electron beam therapy is used in the treatment of superficial tumors like cancer of skin regions and diseases of the limbs. The fast electrons directly ionize the DNA molecule, causing damage. These include single-strand breaks and double-strand breaks, DNA–DNA or DNA–protein cross-links [7]. The usage of the porphyrin-based Photodynamic Therapy (PDT) in conjunction with electron beam radiation therapy can be one of the effective treatment methods for cancer [13–15]. The AREAL 3–4 MeV electron beam has been used to examine the DNA damage in the presence of porphyrins.

The samples (calf thymus DNA and TOEPyP4 porphyrins complexes) with different relative concentrations of porphyrins per base pair were irradiated by the electron beam. After samples irradiation, the melting curves (the dependence of denaturated DNA percentage on temperature) of investigated complexes have been obtained. As the melting temperature of DNA is sensitive to double helix stability, it can be used as an indicator of strand breaks of DNA molecules after radiation. The irradiation caused the DNA structural changes (double-strand breaks or local melting), as expected. At the same radiation dose, the porphyrin high relative concentration causes a stronger radiation effect on the DNA structure. In vitro investigations of DNA damage for various porphyrin concentrations, DNA sequences and radiation dose levels are planned.

4. Applications in materials sciences

4.1. Ferroeletric thin films

Ferroelectric thin films are widely used in memory devices, tunable capacitors, infrared detectors, microactuators, and biochemical sensors, etc. [16,17]. The electric, dielectric, and ferroelectric properties are important characteristics of these thin films and can be modified under electron irradiation leading to films new performance [18–22]. The Ba, Sr, Ti (BST) or Pb , Zr, Ti (PZT) based thin films have wide applications in multifunctional microelectronic devices. The BST thin films have a low frequency dependence of the relative permittivity and dielectric losses, while PZT thin films have a strong dependence of the relative permittivity and dielectric losses from frequency. Those dependences can be substantially changed by the samples electron irradiation producing thin films with the properties tailored to the requirements

Please cite this article as: V.M. Tsakanov, et al., Nuclear Instruments & Methods in Physics Research A (2016), http://dx.doi.org/10.1016/j.nima.2016.02.028

of the application. The 4 MeV electron beam irradiation effects on the electric, dielectric, and ferroelectric properties of the (Ba,Sr) TiO_3 film-based chip sensor with Pt interdigitated electrodes (Fig.5) have been studied in the frequency range from 100 Hz to 1 MHz. As an example, Fig. 6 presents the dielectric permittivities versus frequency dependence before and after irradiation. As is seen, after irradiation the dielectric permittivity ε goes down shifting to the low frequency range. The study of frequency dependence of BST and PZT thin films capacitance, dielectric permittivity, and loss tangent under various electron irradiation conditions are foreseen.

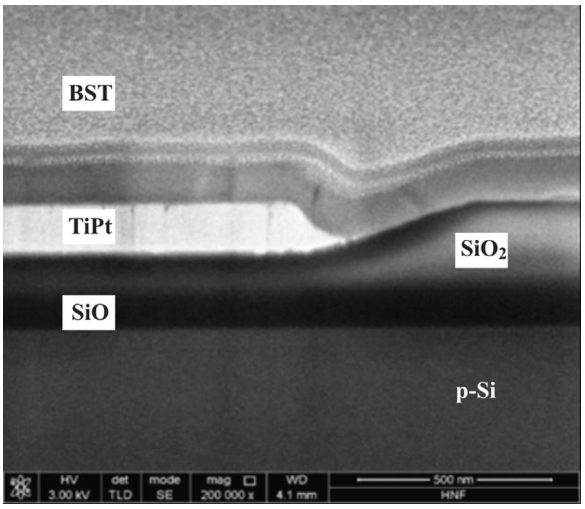

Fig. 5. Cross-sectional SEM image of the chip showing the Si–SiO_2–Ti–Pt BST layer stack.

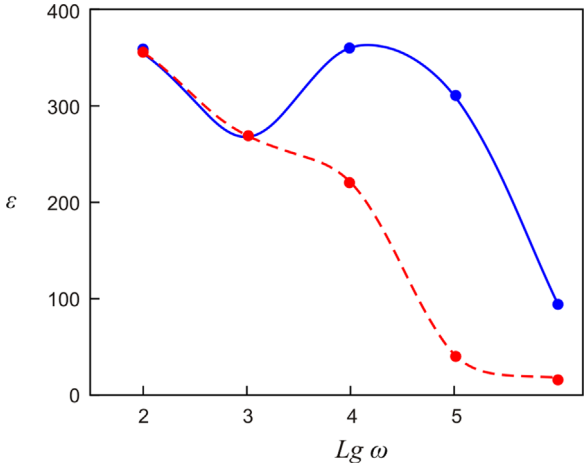

Fig. 6. Dielectric permittivity ε of the sample before (solid) and after irradiation (dashed).

4.2. Silicon and silicon-dielectric structures

Increasing demands for materials and devices applied in modern science and technology stipulate interest in physical properties depending on external influences, e.g. irradiation. The nature of observed physical phenomena strongly depends on structural defects of materials (displaced atoms in crystal lattice, impurity centers, etc.) [23–27].

The behavior of silicon and silicon-dielectric structures, which are the basic elements of modern microelectronic industry, were studied under AREAL ultrashort duration (0.4 ps), high peak current (0.5 kA), 3.5 MeV energy electron beam irradiation. It is well known that the crystals irradiation with electrons of energy less than 10 MeV mainly causes point pair defects. In the case of high electron beam pulse intensity one can expect cluster defects or disordered region formation. The temperature dependence of the carrier concentration n and mobility μ (Fig. 7) has been analyzed before and after irradiation for n-type silicon crystal with a resistivity of 100 Ω cm. From carrier concentration (Fig. 7, left) one can calculate the activation energy $\Delta E = 0.18$ eV (the so-called "A-center"). The activation energy in this case means the energy from the position of a given level to the bottom of the conduction band in the forbidden gap of the silicon zone structure.

A significant decrease in carrier concentration after irradiation is observed (Fig. 7, left), which refer to deeper energetic levels of other radiation defects with higher concentration. The analysis of temperature dependence of carrier mobility (Fig. 7, right) sheds light upon the scattering mechanism of the carriers, i.e. the physical nature of radiation defects. The graphics show the presence of two scattering laws corresponding to two energetic levels, assumedly, A-centers and their clusters. To support this statement, another sample of n-type silicon crystal with resistivity of 700 Ω cm was studied where the carrier concentration is much less and hence does not hinder the observation of scattering process. It was observed that the difference between carrier concentrations before and after irradiation is an order of magnitudes, and the carrier mobility decreased twice even at room temperature, which describes the behavior of clusters radiation defect formation [27].

4.3. Crystals for inorganic scintillators

Inorganic scintillators have various fields of applications including nuclear medicine and high energy physics. The development of new

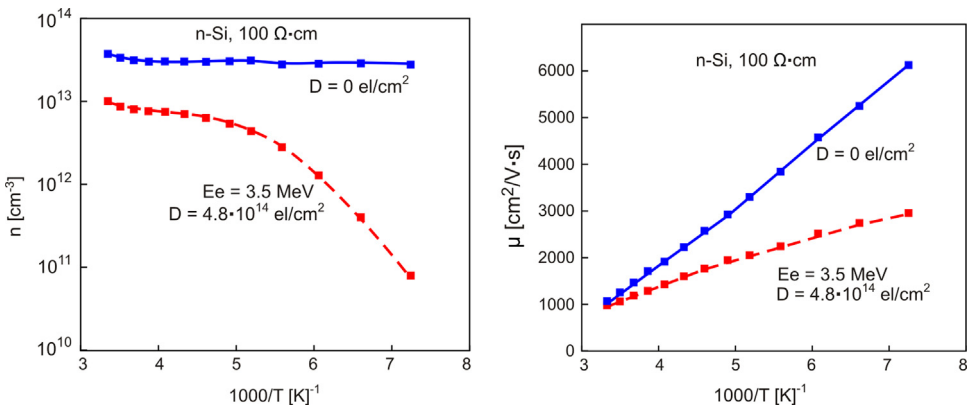

Fig. 7. Temperature dependence of majority carrier concentration (left) and carrier mobility (right) for n-Si of specific resistance 100 Ω cm before and after irradiation.

inorganic scintillators for high energy physics detectors involves the study of radiation hardness crystals. Scintillators based on lutetium aluminum garnet ($Lu_3Al_5O_{12}$ or LuAG) with various activators are in the list of promising candidates for these applications, along with bismuth germinate ($Bi_4Ge_3O_{12}$ or BGO), lead tungstate ($PbMoO_4$ or PWO) and others [28–31]. The required radiation tolerances to these scintillator materials are that after an integrated dose of 1 MGy, the degradation of optical transmittance is limited to 10%. A 5 MeV energy AREAL accelerator can be applied for systematic study of new material radiation tolerances. The irradiation tests of the crystals may contribute to deeper understanding of crystals defects origin in ppm levels. The first irradiation tests on LuAG:Ce and LuAG:Pr single crystals with applied doses of 1–1.5 kGy have been carried out at the AREAL facility. Fig. 8 shows the optical transmission of one of LuAG:Ce samples measured before and after the irradiation with applied dose of 1.5 kGy. The 520–550 nm range is most important, since the emission peak of this scintillator is at 520 nm. Degradation of the optical transmission in this range is limited to less than 1% for the applied dose of 1–1.5 kGy. The study of various crystal compositions in wide irradiation dose range is underway.

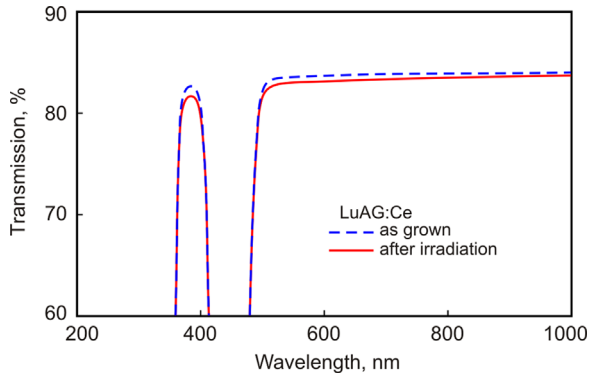

Fig. 8. The optical transmission of LuAG:Ce crystal before (dashed) and after the irradiation (solid). The applied dose is 1.5 kGy.

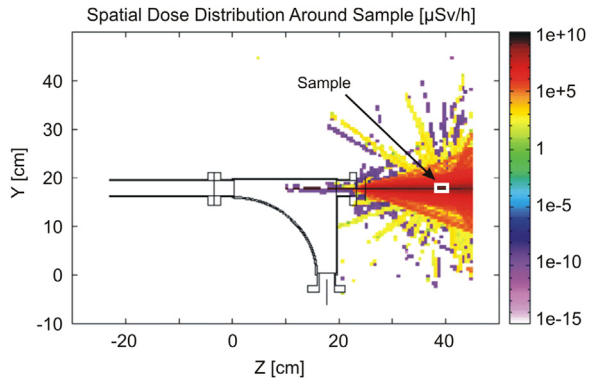

Fig. 9. Radiation field spatial distribution at experimental station H1.

5. Radiation dose distributions

An important issue of the electron irradiation experiments is the spatial and absorbed (by sample) dose distributions. The experimental studies at AREAL have been supported by modeling the dose distributions using the FLUKA [32] code. The numerical simulations have been compared to the measurements. Fig. 9 shows the radiation field spatial distribution (experimental station H1) for the incident electron beam energy of 3.6 MeV and 250 pC charge. As is seen, the radiation is concentrated in the sample region.

The simulated absorbed dose distribution at the experimental station H1 within the biological sample (water equivalent) along the horizontal axis of beam direction is given in Fig. 10a. The calculated total absorbed dose for water-filled cylinder of 1 cm diameter and 2 cm length is 0.37 Gy, while the measured ambient dose equivalent in the vicinity of the biological sample is 0.34 Gy. The simulated and measured absorbed doses coincide within 10%.

The absorbed dose distribution within the semiconductor sample along the horizontal axis pointing to beam direction is shown in Fig. 10b. The spike of the graph corresponds to $Ba_{25}Sr_{75}TiO_3$ film-based chip.

6. Summary

The first results of the AREAL 2–5 MeV energy electron beam applications in diverse fields of life and materials sciences were presented. The analysis shows the potential of facility applications in the fields of radiobiology, molecular physics, solid-state physics, and microelectronics. The AREAL further experimental program anticipates the study of gaps formation in the DNA repair process, normal and human cancer cell behavior under irradiation, irradiation in-situ effects in silicon crystals and ferroelectrics, the study of radiation hardness scintillators crystals.

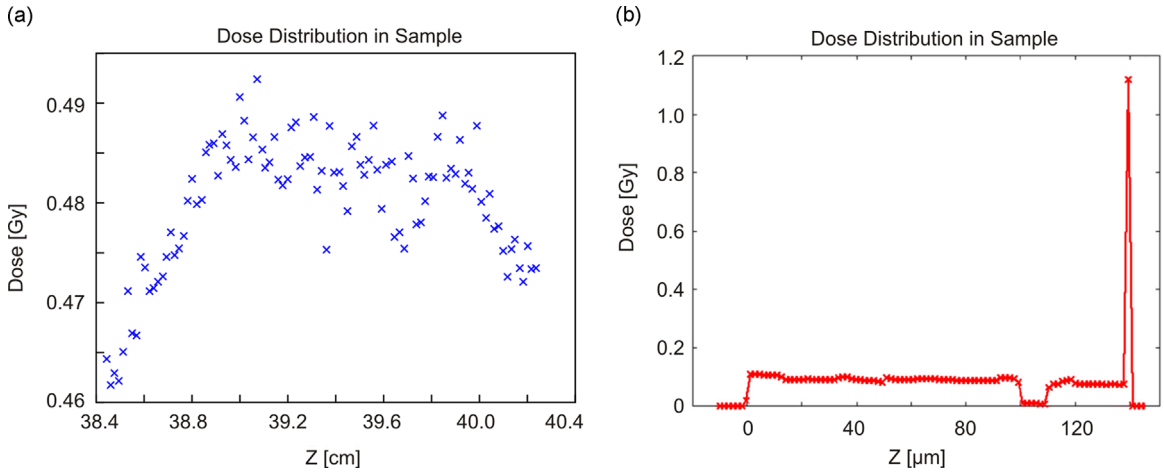

Fig. 10. Simulated absorbed dose distributions for the biological (a) and semiconductor (b) samples.

Please cite this article as: V.M. Tsakanov, et al., Nuclear Instruments & Methods in Physics Research A (2016), http://dx.doi.org/10.1016/j.nima.2016.02.028

ARTICLE IN PRESS

Acknowledgments

The experimental studies were conducted within the framework of RA MES State Committee of Science Projects no. 14AR-1f06, 14AR-1c02, 14AR-2f12 (bio-medical applications, ferroelecric films, and silicon structures) and Project 644260-INTELUM-H2020-RISE-2014 (crystals for inorganic scintillators).

References

[1] B. Grigoryan et al., in: Proceedings of the IPAC2014, Dresden, Germany, 2014, pp. 620.
[2] K. Floettmann, Nuclear Instruments and Methods in Physics Research A 740 (2013) 34.
[3] P. Zhu, et al., New Journal of Physics 17 (2015) 063004.
[4] W.L. Santivasi, Xia Fen, Antioxidants and Redox Signaling 21 (2) (2014) 251.
[5] L. Laschinsky, M. Baumann, et al., Journal of Radiation Research 53 (2012) 395.
[6] C. von Sonntag, The Chemical Basis of Radiation Biology, Taylor & Francis, London; Philadelphia, PA, 1989.
[7] P. Swiderek, Angewandte Chemie International Edition 45 (2006) 4056.
[8] N.P. Singh, M.T. McCoy, R.R. Tice, E.L. Schneider, Experimental Cell Research 175 (1988) 184–191.
[9] H. Nikjoo, P. O'Neill, W.E. Wilson, D.T. Goodhead, Radiation Research 156 (5 (Part 2)) (2001) 577.
[10] D.T. Goodhead, International Journal of Radiation Biology 65 (1) (1994) 7.
[11] J.F. Ward, Progress in Nucleic Acid Research Molecular Biology 35 (1988) 95.
[12] M. Kramer, W.K. Weyrather, M. Scholz, Technology in Cancer Research and Treatment 2 (5) (2003) 427.
[13] M.B. Vrouenraets, G.W. Visser, G.B. Snow, G.A. van Dongen, Anticancer Research 23 (1B) (2003) 505.
[14] B.C. Wilson, Canadian Journal of Gastroenterology 16 (6) (2002) 393.
[15] A.E. O'Connor, W.M. Gallagher, A.T. Byrne, Photochemistry and Photobiology 85 (2009) 1053.
[16] A.K. Tagantsev, et al., Journal of Electroceramics 11 (2003) 5.
[17] S.Sh. Gevorgian, Ferroelectrics in Microwave Devices, Circuits and Systems, Springer-Verlag, London, 2009, (394 pp.).
[18] S. Aparna, V.M. Jali, G. Sanjeev, et al., Bulletin Materials Science 33 (3) (2010) 191.
[19] V.A. Balakin, et al., Pisma JTF 29 (2003) 77.
[20] C.M. Othon, S. Ducharme, Ferroelectrics 304 (2004) 9.
[21] C.M. Othon, F.B. Bateman, S. Ducharme, Journal of Applied Physics 98 (2005) 014106.
[22] I. Baturin, et al., Materials Science and Engineering B 120 (2005) 141.
[23] C. Leroy, P.G. Rancoita, Reports on Progress in Physics 70 (4) (2007) 493.
[24] S. Duzellier, Aerospace Science and Technology 9 (2005) 93.
[25] V.V. Emtsev, P. Ehrhart, D.S. Poloskin, K.V. Emtsev, Journal of Material Science: Materials in Electronics 18 (N7) (2007) 711.
[26] N. Nagai, M. Sumitomo, M. Imaizumi, R. Fukasawa, Semiconductor Science and Technology 21 (2006) 201.
[27] H.N. Yeritsyan, et al., Physical Science International Journal 4 (9) (2014) 1225.
[28] P. Lecoq, A. Annenkov, A. Gektin, M. Korzhik, C. Pedrini, Inorganic Scintillators for Detector Systems, Springer-Verlag, Berlin Heidelberg (2006), p. 251.
[29] P. Lecoq, Journal of Physics: Conference Series 160 (2009) 012016.
[30] M.V. Derdzyan, et al., Journal of Crystal Growth 361 (2012) 212.
[31] A.G. Petrosyan, et al., Journal of Crystal Growth 430 (2015) 46.
[32] A. Ferrari, P.R. Sala, A. Fassò, J. Ranft, FLUKA: a multi-particle transport code, CERN 2005-10, 2005.

Please cite this article as: V.M. Tsakanov, et al., Nuclear Instruments & Methods in Physics Research A (2016), http://dx.doi.org/10.1016/j.nima.2016.02.028